Climate Dynamics
https://doi.org/10.1007/s00382-022-06374-2

Roles of climate feedback and ocean vertical mixing in modulating global warming rate

Haijun Yang[1,2] · Xiangying Zhou[1] · Qianzi Yang[3,4] · Yang Li[3]

Received: 30 August 2021 / Accepted: 27 May 2022

Abstract
Despite the rapid increase of greenhouse gases (GHGs) in the atmosphere during the past 50 years, observed global mean surface temperature (GMST) showed a pause in the warming trend during the first decade of the twenty-first century. This is referred to as the global warming "hiatus". A dominant hypothesis emphasizes that the superimposition of the cold phase of the Pacific decadal variability and the global warming trend can lead to the hiatus. Using simply energy balance models, we explore two potential mechanisms that may supress the GMST warming trend: enhanced negative climate feedback and downward heat mixing. Forced by linearly increasing heating, a stronger negative climate feedback can reduce the GMST warming rate, but cannot result in a warming hiatus. Downward mixing of heat can cause a short-lived hiatus of surface warming rate due to enhanced nonlinear ocean heat uptake by the lower ocean, but the surface warming would be accelerated in the long run due to the decline of downward heat mixing rate. This study provides further evidence, both theoretically and numerically, that in the long run, the only route to contain the global warming effectively is to reduce GHG emissions.

Keywords Global warming hiatus · Climate feedback · Vertical mixing

1 Introduction

The increase of greenhouse gases (GHGs) in the atmosphere is commonly thought as the deterministic cause for the centennial warming trend of global mean surface temperature (GMST) since the Industrial Revolution (IPCC 2013). With the steep increase of carbon dioxide (CO_2) in the atmosphere since 1960, the GMST, however, showed a warming pause for about 10 years during the first decade of the twentieth-one century (Fig. 1) (Easterling and Wehner 2009; Knight et al. 2009; Trenberth and Fasullo 2013). This phenomenon is termed as the global warming "hiatus" (IPCC 2013; Kosaka and Xie 2013; Yan et al. 2016). The observed CO_2 concentration at Mauna Loa of Hawaii has exceeded 400 ppm since 2015 (Fig. 1), with a growth rate of annual mean CO_2 at Mauna Loa being about 2 ppm/year since 2000, well above any preceding period. This inconsistency between the warming hiatus and the intensification of anthropogenic forcing has set off fierce scientific and political debates on the authenticity of global warming.

A global warming hiatus can appear when the warming trend encounters natural climate variability. This mechanism was first proposed by Kosaka and Xie (2013), and recognized by many scientists (Clement and DiNezio 2014; England et al. 2014; Dai et al. 2015). In Kosaka and Xie (2013), the global warming hiatus was well simulated after nudging the model sea-surface temperature (SST) to the observed SST in the central to eastern tropical Pacific in a historical run. Xie et al. (2016) further indicated that the temporal variation of SST can be driven by radiative forcing and periodic natural variability. When the natural variability happens to be in a downward phase, the warming hiatus would occur. The natural variability is widely believed to be the

✉ Haijun Yang
yanghj@fudan.edu.cn

1 Department of Atmospheric and Oceanic Sciences and Institute of Atmospheric Science and CMA-FDU Joint Laboratory of Marine Meteorology, Fudan University, 2005 Songhu Road, Shanghai 200438, China

2 Shanghai Scientific Frontier Base for Ocean-Atmosphere Interaction Studies, Fudan University, Shanghai 200438, China

3 Department of Atmospheric and Oceanic Sciences, School of Physics, Peking University, Beijing 100871, China

4 Present Address: Shenzhen Middle School, 1068 West Nigang Road, Luohu District, Shenzhen, Guangdong 518024, China

Published online: 26 June 2022

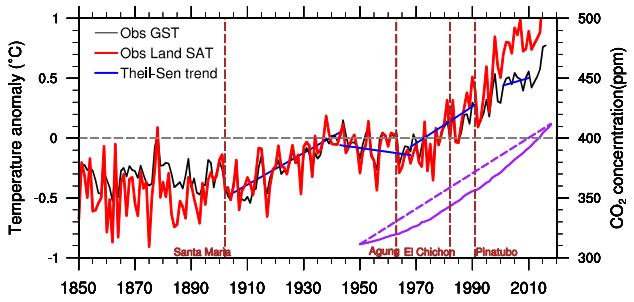

Fig. 1 Time series of observed global mean surface temperature (GMST) (black; units: °C), global mean land surface temperature (red; units: °C) and CO_2 concentration (purple; units: ppm). The climatological mean state of 1960–1990 is removed from the temperature. Segments of blue line show the linear trends of GMST in different periods. Dashed vertical lines denote four serious volcanic events: Santa Maria in 1902, Agung in 1963, El Chichon in 1982, and Pinatubo in 1991. Dashed purple line shows the linear trend of CO_2 concentration. The surface temperature data is from the HadCRUT4 (Jones et al. 2012; Morice et al. 2012), downloaded at https://crudata.uea.ac.uk/cru/data/temperature/. The CO_2 data is from the station at Mauna Loa of Hawaii, downloaded at https://gml.noaa.gov/ccgg/trends/

Pacific decadal oscillation (PDO) (Clement and DiNezio 2014; Dai et al. 2015). The recent hiatus appeared because the historical SST happened to be in the cold phase of the PDO during the first decade of the twentieth-one century (Meehl et al. 2013; Trenberth and Fasullo 2013; Brown et al. 2015). This kind of hiatus also occurred during1943–1976 (Fig. 1) (Trenberth and Fasullo 2013; England et al. 2014), when the PDO was in its cold phase. Although about 30% of heat uptake increase occurs in the eastern tropical Pacific associated with the cold phase of the PDO, studies also suggested that the Pacific was not the only contributor to the hiatus, and other ocean basins, in particular, the southern and subtropical Indian Ocean and subpolar North Atlantic, contributed substantially to the global warming hiatus via reduced heat loss to the atmosphere (Drijfhout et al. 2014).

A more intuitive explanation to the recent GMST hiatus comes from the view of Earth's energy budget: either a reduction in radiative forcing from the top of the atmosphere (TOA) or an enhanced heat uptake by the deeper ocean (Tung and Chen 2018) could lead to a hiatus. Weakened solar radiation during a period of low sunspot activity (Trenberth 2009), or due to reduction in stratospheric water vapor (Solomon et al. 2010), and increasing aerosols related to anthropogenic activities (Smith et al. 2016; Kaufmann et al. 2011) and 17 small volcano eruptions since 1999 (Santer et al. 2014; Smith et al. 2016) could have contributed to the recent hiatus by weakening the net TOA incoming energy. Trenberth and Fasullo (2013) showed that forcing reductions from these factors likely contributed no more than 20% of the global warming slowdown. Schmidt et al. (2014) showed that recent moderate volcano eruptions and anthropogenic pollutions accounted for half of the divergence between observation and model simulations, while the solar minimum explained one seventh. Kühn et al. (2014) found that Asian pollution from coal burning has very little effect globally or regionally, because of the cancelation between the warming effect of black carbon and the cooling effect of sulphate aerosols.

The net TOA energy gain during the recent hiatus is estimated to be $0.5 \pm 0.43\,\mathrm{W}/m^2$ (Loeb et al. 2012), showing no apparent reduction. The deep ocean is thus emerged as a likely candidate to absorb the additional energy, buffering the global warming and leading to the GMST hiatus (Meehl et al. 2011; Balmaseda et al. 2013a, b; Rhein et al. 2013; Liu et al. 2016). Both observations and model simulations showed that the vertical heat redistribution, especially in the North Atlantic and Southern Ocean, is remarkably different between hiatus period and fast-warming period (Meehl et al. 2011; Chen and Tung 2014; Drijfhout et al. 2014; Liu et al. 2016). The subsurface warming in the Southern Ocean is attributed to the southward displacement and intensification of the circumpolar jet, while the North Atlantic's role is believed to be related to the Atlantic meridional overturning circulation (AMOC). Meehl et al. (2011) simulated a negative trend of the AMOC in a historical run, that is, a weakening of deep convection in the North Atlantic, which can lead to subsurface warming. In contrast, Chen and Tung (2018) showed an acceleration of the AMOC during 1993–2005 based on various independent proxies. They believed that the enhanced deep convection transports more heat downward to the deep ocean, which neutralizes the warming effect caused by human activities and slows down the surface warming.

In this work we explore theoretically whether the Earth's warming trend as a whole can be controlled under a linear increase of GHGs. Using simple energy balance models (EBMs), we examine two candidates: the overall global climate feedback and ocean vertical mixing. From the viewpoint of Earth energy balance, a stronger negative climate feedback would reduce the net energy absorbed by the Earth surface, which might have the potential to control the GMST warming. However, in reality the global climate feedback is getting even positively stronger (Armour et al. 2013; Gregory et al. 2015; Rugenstein et al. 2020), which would potentially result in a disastrous runaway warming. Enhanced ocean vertical mixing can reduce the global warming rate over a short term, by mixing heat downward to the deeper ocean; however, it would eventually accelerate the surface warming in the long run, once the deeper ocean is saturated. A stronger overturning circulation can also transport more surface warm water downward, contributing to the hiatus over a short time. However, the overturning circulation itself depends strongly on the stratification, and can be shut down by a reduced stratification. This study provides further

evidence that in the long run, the only route to contain the global warming effectively is to reduce GHGs, namely, to change the behaviour of human beings.

This paper is organized as follows. In Sect. 2, we introduce one-box EBMs, and investigate the role of climate feedback in the hiatus of global warming rate. Two-box model is introduced in Sect. 3, and the role of vertical ocean mixing is examined. Summary and discussion are given in Sect. 4. Detailed derivation of theoretical equations is provided in an Appendix.

2 One-box model with climate feedback

First, we use a zero-dimensional EBM, i.e., a 1-box ocean model (Fig. 2a), to investigate the impact of climate feedback on surface warming trend. The transient response of the GMST in the 1-box model is proportional to the net energy flux at the TOA (Gregory et al. 2004), that is,

$$C\frac{d\Delta T}{dt} = F - B\Delta T, \tag{1}$$

where $C = \rho c_p D$ is ocean heat capacity, $\rho = 1026\,kg \bullet m^{-3}$ is seawater density, $c_p = 3900J \bullet (kg°\mathrm{C})^{-1}$ is seawater specific heat at constant pressure, and D is ocean depth, set to 400 m here. Symbol Δ denotes the anomaly from the equilibrium climate. F is the anomalous radiative forcing at the TOA, caused by changes of GHGs. B is the climate feedback parameter for the Earth as a whole. In this paper, positive (negative) B denotes negative (positive) feedback. B must be positive so that the system can reach a stable state. Bloch-Johnson et al. (2015) estimated that the reasonable range of B is $0.8 - 1.8W \bullet m^{-2}K^{-1}$, based on the abrupt $4\times CO_2$ experiments of the Coupled Model Inter-comparison Project Phase 5 (CMIP5). In this work, $B = 1.5W \bullet m^{-2}K^{-1}$.

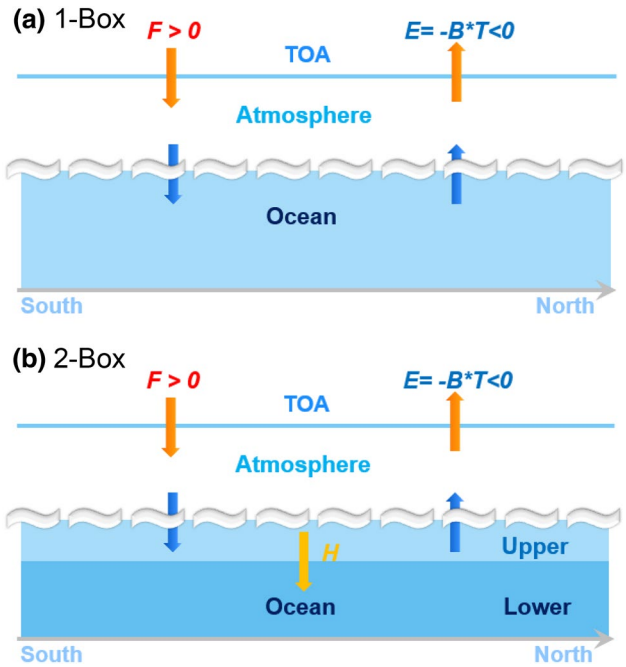

Fig. 2 Schematic diagrams of box models: (**a**) 1-box ocean model and (**b**) 2-box ocean model. In all box models, the net radiation flux at the top of the atmosphere (TOA) is $F+E$, each shown by an orange arrow. The ocean surface heat flux is denoted by solid blue arrows. In (**b**), yellow arrow represents vertical heat transport in the ocean interior

Usually, F should be zero in an equilibrium climate state, and temperature stays unchanged. However, if the GHGs increase, the Earth gains extra energy that causes ΔT to increase. Here, we assume the concentration of GHGs increases linearly with time, and the anomalous radiative forcing can be simply expressed by:

$$F = \varepsilon t, \tag{2}$$

where ε is set to $0.016W \bullet m^{-2}yr^{-1}$, which is equivalent to the greenhouse effect by a gradual doubling of CO_2 concentration over 200 years.

2.1 Constant climate feedback

The situation with constant climate feedback is examined first. Under a linearly increasing radiative forcing given in Eq. (2), the theoretical solution to Eq. (1) can be easily written as follows,

$$T = \frac{\varepsilon}{B}\left[t - \frac{C}{B}\left(1 - e^{-\frac{B}{C}t}\right)\right]. \tag{3}$$

For simplicity, ΔT is written as T from now on. Thus, the warming rate is,

$$\frac{dT}{dt} = \frac{\varepsilon}{B}\left(1 - e^{-\frac{B}{C}t}\right), \tag{4}$$

When $t \to \infty$, the ocean warming goes toward infinity, and the warming rate reaches a constant $\frac{\varepsilon}{B}$, that is,

$$T = \frac{\varepsilon}{B}\left(t - \frac{C}{B}\right) \to \infty, \frac{dT}{dt} = \frac{\varepsilon}{B}, \text{when} t \to \infty. \tag{5}$$

Here, we can define the e-folding timescale $\tau = \frac{C}{B}$, to represent the fast transient timescale of the surface warming (Hansen et al. 1981), which is about 34 years here. When $t > \tau$, the surface warming goes up roughly linearly and the warming rate approaches a constant.

Figure 3a, b show the theoretical solutions of T and $\frac{dT}{dt}$, respectively. T increases roughly linearly as expected (Fig. 3a). During the first several decades, the warming rate ($\frac{dT}{dt}$) itself increases roughly linearly, and then reaches a constant value in about 100 years (Fig. 3b). The ocean temperature eventually increases linearly after 100 years (Fig. 3a), and the system will never reach an equilibrium. Of course,

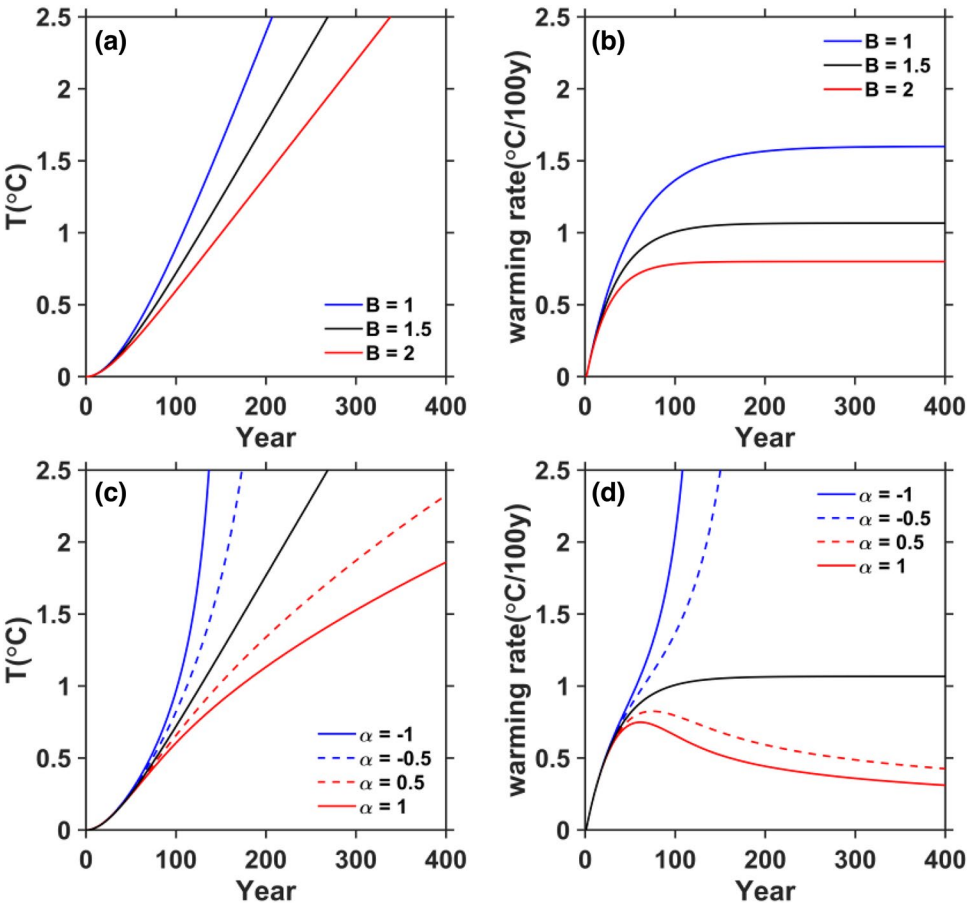

Fig. 3 Temporal changes of ocean temperature (units: °C; left panels) and warming rate (units: °C/100-year; right panels) in 1-box model. Top panels are for constant climate feedback (B; units: $W \bullet m^{-2}K^{-1}$), and B is set to 1.0 (blue), 1.5 (black) or 2.0 (red). Bottom panels are for varying B, where B decreases (blue) or increases (red) with temperature at a rate of -1.0 or -0.5 ($+1.0$ or $+0.5$) $W \bullet m^{-2}K^{-2}$. Black line is for the control case with constant B (1.5)

stronger negative feedback will lead to a weaker warming rate, and vice versa (color curves, Fig. 3a, b). The temperature change is straightforward under the constant climate feedback. One important implication here is that to bend the warming rate curve downward, i.e., to reduce the warming rate to zero, or in other words, to realize a global warming hiatus in this simple box model, an extremely strong negative feedback is required. In fact, Eq. (5) shows that only when $B \to \infty$, $\frac{dT}{dt} = \frac{\epsilon}{B} \to 0$. This situation is practically impossible.

2.2 Varying climate feedback

Here, we explore the possibility of a global warming hiatus by assuming a temperature-dependent climate feedback,

$$B = B_0 + \alpha T, \tag{6}$$

where $B_0 = 1.5\, W \bullet m^{-2}K^{-1}$ is the reference climate feedback from an unperturbed state, and α represents the rate of climate feedback change (units: $W \bullet m^{-2}K^{-2}$). A positive (negative) α means that the climate feedback becomes more negative (positive) with global warming. Under the situation (6), Eq. (1) is a quadratic equation, so that the curves for warming (T) and warming rate ($\frac{dT}{dt}$) can be bent downward under a strong positive α. This situation was studied previously (e.g., Winton et al. 2010; Armour et al. 2013; Bloch-Johnson et al. 2015; Gregory et al. 2015).

The theoretical solution to system (1), (2) and (6) is written as follows,

$$T(t) = \frac{aKm\left[A(1,M) + \frac{K_1}{K_2}A(3,M)\right] - \frac{b}{2}\left[A(0,M) + \frac{K_1}{K_2}A(2,M)\right]}{a\left[A(0,M) + \frac{K_1}{K_2}A(2,M)\right]}, \tag{7}$$

where $M = m(\frac{b^2}{4} + aKt)$, $m = (aK)^{-\frac{2}{3}}$ and $A(i,M)$ is the Airy function (Abramowitz and Stegun 1964). There are four kinds of Airy function. $A(1,M)$ is the derivative of $A(0,M)$, and $A(3,M)$ is the derivative of $A(2,M)$. Details on the derivation of Eq. (7) and parameters K, K_1, K_2, a and b can be found in Appendix.

For the Airy functions, we have,

$$\begin{cases} A(0,M) = \frac{e^{-\frac{2}{3}M^{\frac{3}{2}}}}{2\pi^{\frac{1}{2}}M^{\frac{1}{4}}} \to 0, A(1,M) = -\frac{M^{\frac{1}{4}}e^{-\frac{2}{3}M^{\frac{3}{2}}}}{2\pi^{\frac{1}{2}}} \to 0 \\ A(2,M) = \frac{e^{\frac{2}{3}M^{\frac{3}{2}}}}{\pi^{\frac{1}{2}}M^{\frac{1}{4}}} \to \infty, A(3,M) = \frac{M^{\frac{1}{4}}e^{\frac{2}{3}M^{\frac{3}{2}}}}{\pi^{\frac{1}{2}}} \to \infty \end{cases}, \text{when } t \to \infty. \tag{8}$$

Therefore,

$$\begin{cases} T = -\frac{b}{2a} + \left(\frac{b^2}{4a^2} + \frac{K}{a}t\right)^{\frac{1}{2}} \to \infty \\ \frac{dT}{dt} = Kt - (b + aT)T \to 0 \end{cases}, \text{when } t \to \infty. \quad (9)$$

The global warming will slow down and the warming rate will reduce substantially if the negative climate feedback increases with the global warming (i.e., $\alpha > 0$) (red curves, Fig. 3c, d). However, a global warming hiatus, i.e., the zero warming rate, appears to be unlikely for a reasonable range of the climate feedback. In contrast, the global warming will be easily out of control if the negative feedback is weakened by the global warming (i.e., $\alpha < 0$) (blue curves, Fig. 3c, d). This is also called "quadratic runaway" (Bloch-Johnson et al. 2015). To view clearly the temperature change, we examined the situations with $\alpha = \pm 0.5, \pm 1.0\, W \bullet m^{-2}K^{-2}$. These values are extremely strong when compared to more practical values derived from observations and coupled models. For example, based on estimates from various coupled model studies, α is suggested to be in the range of $\pm 0.06\, W \bullet m^{-2}K^{-2}$ (Roe and Armour 2011). Previous studies suggested that the Planck feedback would become more negative under the global warming, at a rate of about $0.02\, W \bullet m^{-2}K^{-2}$ (Bloch-Johnson et al. 2015). The water vapour feedback would become more positive, possibly offsetting the negative lapse rate feedback (Bony et al. 2006; Soden and Held 2006). The surface albedo feedback would be weakened with the melting of snow and ice under global warming, that is, this negative feedback will, in fact, become weaker, at a rate of about $0.1\, W \bullet m^{-2}K^{-2}$(Manabe and Bryan 1985). In Fig. 3c, d, the black and red curves are plotted based on the theoretical solution (7), while the blue curves are plotted based on numerical solutions to Eq. (A1) (Appendix), since the Airy function does not work very well when $\alpha < 0$.

In fact, Eq. (9) suggests that, when the time goes to infinity, the warming magnitude itself goes to infinity, while the global warming rate could approach zero. To show this situation more clearly, we replot the temperature and its rate of change in the case of $B = 1.5, \alpha = 1.0$ in Fig. 4. We can see that in about 10^5 years, the warming rate can approach zero (it would never be equal to zero based on Eq. (A1)), the global ocean warming can be as strong as 40 °C. Of course, this situation is far beyond the reality, even for the Earth's climate over the past billion years. Therefore, we can conclude safely that it is unlikely to obtain a global warming hiatus by merely enhancing the negative feedback, in the case of linearly increasing external forcing. We can expect a substantial slowdown of the global warming under strong negative feedback, but never the zero warming rate (hiatus). Moreover, even under an extremely strong negative feedback, the mitigation effect of climate feedback works slowly at inter-decadal to centennial timescales (Fig. 3d). Figure 3 suggests that it is unlikely that the climate feedback change alone has contributed seriously to the GMST hiatus observed in the first decade of the twenty-first century century.

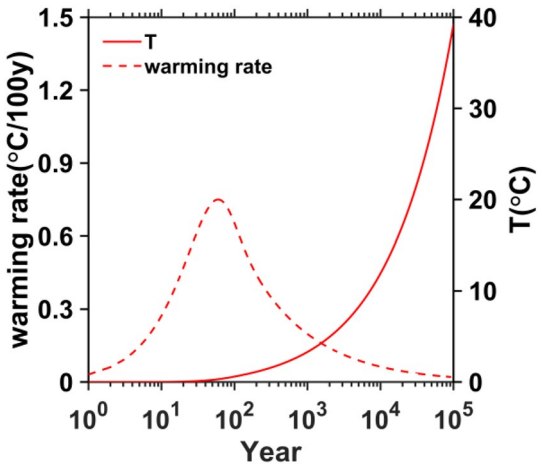

Fig. 4 Temporal changes of ocean temperature (units: °C; solid red) and warming rate (units: °C/100-year; dashed red) in 1-box model, under the situation with strong nonlinear climate feedback ($B = 1.5$ and $\alpha = 1.0$)

3 Two-box model with vertical heat mixing

As the 1-box EBM does not take into account ocean interior process, a 2-layer ocean EBM is introduced here to study the effect of lower ocean on the surface warming (Fig. 2b). Due to its enormous heat capacity, the interior ocean could play a role in GMST hiatus, by taking up heat from the layer above and redistributing the heat in the vertical (Gregory 2000). The 2-layer box model is widely used in the study of transient climate responses (e.g., Held et al. 2010; Geoffroy et al. 2013; Zhou and Chen 2015; Yoshimori et al. 2016), climate sensitivity (Gregory et al. 2015), and so on. The model is effective in capturing the minimal physics of transient surface temperature change (Gregory et al. 2015).

The 2-layer model consists of upper and lower oceans (Fig. 2b), and the layers have heat capacities C_1 and C_2, respectively. Here, we set $C_2 = 10C_1$, corresponding to a 400-m upper ocean and a 4000-m lower ocean, respectively. The upper ocean participates in the surface energy budget, and transports heat flux $H = \gamma(T_1 - T_2)$ downward to the deep ocean through processes such as vertical advection, mixing and diffusion. We simply call them "vertical heat transport" or ocean heat uptake (OHU) by the lower ocean in this work. The model equations are,

$$C_1\frac{dT_1}{dt} = F - BT_1 - \gamma(T_1 - T_2) \tag{10}$$

$$C_2\frac{dT_2}{dt} = \gamma(T_1 - T_2) \tag{11}$$

$$T_v = T_1 - T_2 \tag{12}$$

where T_1 and T_2 are the temperature anomalies of upper and lower layers, respectively, from an unperturbed climate; and T_v is the change in vertical temperature gradient. γ represents the efficiency of vertical heat transport (units: $W \bullet m^{-2}K^{-1}$). It is also treated as the heat uptake efficiency by the deep ocean (Gregory and Mitchell 1997; Gregory et al. 2015). γ can vary empirically over time (Raper et al. 2002). Watanabe et al. (2013) reported a range of γ of about $0.5 - 1.5\ W \bullet m^{-2}K^{-1}$ based on outputs from 16 CMIP5 models. Gregory et al. (2015) used γ of about $0.4 - 0.8\ W \bullet m^{-2}K^{-1}$ in their box models. In this work, we set $\gamma = 0.5\ W \bullet m^{-2}K^{-1}$.

3.1 Constant efficiency of vertical heat transport

The analytical solutions to the 2-box system of (10)-(12) under constant γ are written as follows,

$$T_1(t) = \frac{\varepsilon}{B}[t - \tau_f a_f\left(1 - e^{-\frac{t}{\tau_f}}\right) - \tau_s a_s\left(1 - e^{-\frac{t}{\tau_s}}\right)] \tag{13}$$

$$T_2(t) = \frac{\varepsilon}{B}[t - \varphi_f\tau_f a_f\left(1 - e^{-\frac{t}{\tau_f}}\right) - \varphi_s\tau_s a_s\left(1 - e^{-\frac{t}{\tau_s}}\right)] \tag{14}$$

$$T_v(t) = \frac{\varepsilon}{B}[(\varphi_f - 1)\tau_f a_f\left(1 - e^{-\frac{t}{\tau_f}}\right) + (\varphi_s - 1)\tau_s a_s\left(1 - e^{-\frac{t}{\tau_s}}\right)] \tag{15}$$

The warming rates for the 2-layer ocean are,

$$\frac{\mathrm{d}T_1}{dt} = \frac{\varepsilon}{B}(1 - a_f e^{-\frac{t}{\tau_f}} - a_s e^{-\frac{t}{\tau_s}}) \tag{16}$$

$$\frac{\mathrm{d}T_2}{dt} = \frac{\varepsilon}{B}(1 - \varphi_f a_f e^{-\frac{t}{\tau_f}} - \varphi_s a_s e^{-\frac{t}{\tau_s}}) \tag{17}$$

Here, we have defined the fast transient timescale τ_f and the slow timescale τ_s, respectively, as follows,

$$\tau_f = \frac{C_1C_2}{2B\gamma}\left(b - \sqrt{\delta}\right), and\ \tau_s = \frac{C_1C_2}{2B\gamma}(b + \sqrt{\delta}) \tag{18}$$

Details on the derivation of Eqs. (13, 14, 15, 18), and the parameters therein can be found in Appendix.

Based on (13–15), we have

$$\begin{cases} T_1 = \frac{\varepsilon}{B}\left(t - \frac{C_1+C_2}{B}\right) \to \infty, \\ T_2 = \frac{\varepsilon}{B}\left(t - \frac{C_1+C_2}{B} - \frac{C_2}{\gamma}\right) \to \infty, \\ T_v = \frac{\varepsilon}{B} * \frac{C_2}{\gamma} = finite, \\ \frac{\mathrm{d}T_1}{dt} = \frac{\mathrm{d}T_2}{dt} = \frac{\varepsilon}{B}. \end{cases} \text{when } t \to \infty \tag{19}$$

Under constant γ, the warming rate for the 2-box ocean will eventually approach that of the 1-box ocean (Eq. (5)).

The transient timescales τ_f and τ_s given in Eq. (18) are for the upper and lower oceans, respectively, which are about 25 and 1360 years, respectively, given the parameter $\gamma = 0.5$, $B = 1.5$ and the depths of the 2-box ocean of 400 and 4000 m, respectively. Since we consider a linearly increasing external forcing in this paper, it is the warming rate, instead of warming itself, that can reach the equilibrium. Therefore, τ_f and τ_s can be thought as the e-folding timescales of the warming rate for the upper and deep oceans, respectively. This is *qualitatively* consistent with fast and slow timescales for the temperature changes in a 2-layer ocean, under sudden constant external forcing (Gregory et al. 2015). It is expected that for the lower ocean, the quasi-equilibrium timescale of the warming rate can be as long as several thousand years, under linearly enhancing external forcing.

Figure 5a–c show the results of theoretical solutions (13)-(17). The OHU by the lower ocean can slow down the surface warming. This is straightforward, and can be easily deduced from Eqs. (1) and (10). Under the same external forcing and climate feedback, the surface temperature increase in the 2-box model is smaller in magnitude than that in the 1-box model. For example, at the end of the 200$^{\text{th}}$ year, T_1 in the 2-box model is about 1.4 °C (Fig. 5a), 20% smaller than that in the 1-box model (~ 1.8 °C) (Fig. 3a). Here, $\gamma = 0.5$ and $B = 1.5$. Under the linearly increasing forcing, in the long run (more than 3000 years) the 2-layer system can approach an "equilibrium" state, in terms of warming rate ($\frac{dT}{dt}$) and vertical temperature gradient (T_v) (Fig. 5b, c). The 2-layer ocean will eventually warm up at the same rate $\frac{\varepsilon}{B}$ as indicated in Eq. (19) and shown in Fig. 5b, which is independent of γ. T_v will eventually reach a constant $\frac{\varepsilon}{B} * \frac{C_2}{\gamma}$ (~ 10.8 °C) (Eq. (19), Fig. 5c), which is inversely proportional to γ.

It is obvious that the efficiency of vertical heat transport γ affects the magnitude and timescale of temperature change in each layer. It does not affect those of the whole ocean, since it only redistributes the heat in the vertical. A larger

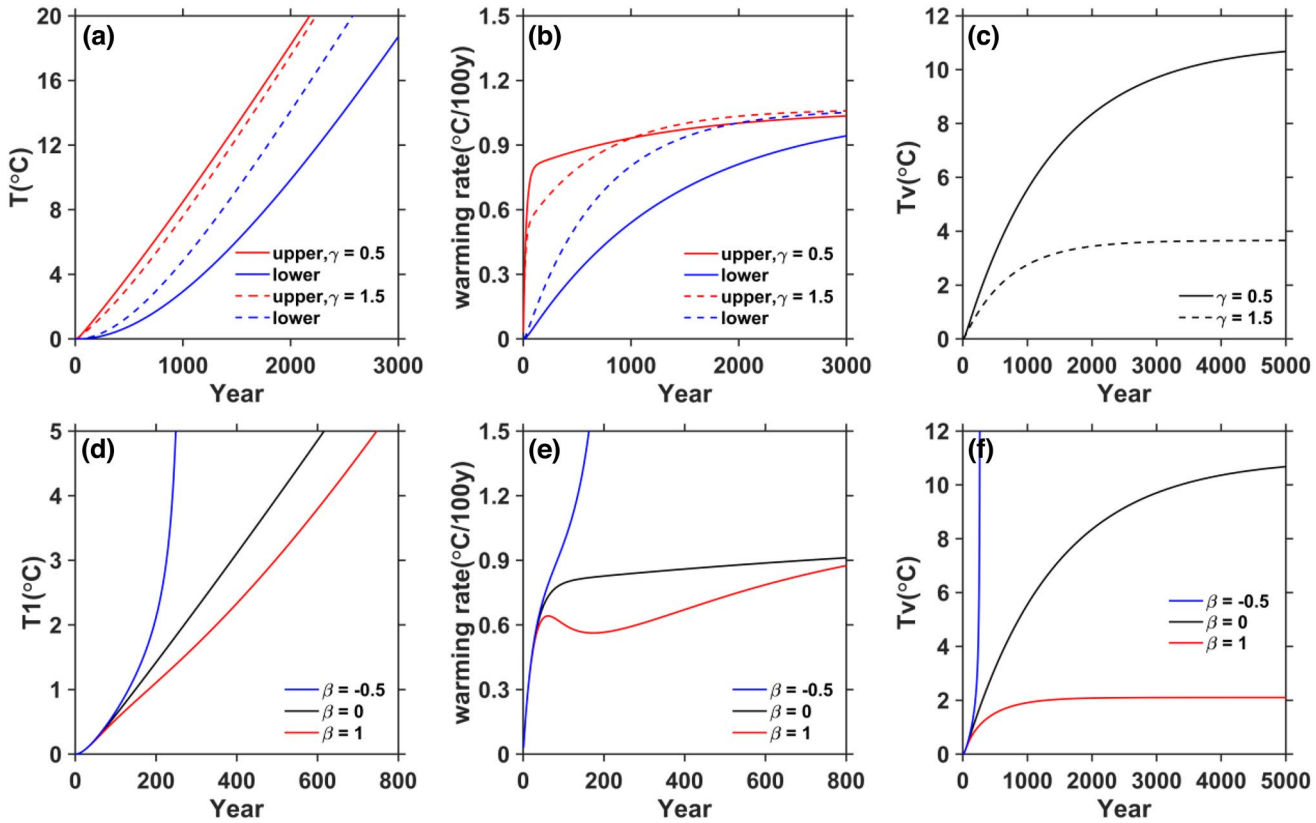

Fig. 5 Temporal changes of ocean temperature (units: °C; left panels), warming rate (units: °C/100-year; middle panels) and ocean stratification (T_v; units: °C; right panels) in 2-box model. In (**a**, **b**), red curves are for upper ocean; and blue curves, for lower ocean. In (**a**–**c**), solid (dashed) curves represent the case when $\gamma = 0.5(1.5)$ $W \bullet m^{-2}K^{-1}$. In (**d**, **e**), only SST changes are plotted. In (**d**–**f**), blue (red) curve is for the case when γ decreases (increases) with T_v at a rate of $-0.5(+1.0)\, W \bullet m^{-2}K^{-2}$. Black curve is for the control case with constant γ (i.e., $\beta = 0$)

γ will lead to a quicker and stronger warming in the deep ocean, at the cost of a slower and weaker warming in the upper ocean (Fig. 5a, b), which leads to a weaker vertical temperature gradient (dashed black, Fig. 5c). The theoretical solution (Eq. (19)) shows that the equilibrium warming rates for both the surface and deep oceans depend only on the external heating rate (ε) and the overall climate feedback (B) of the system, regardless of the interior parameters of the ocean. The overall warming magnitude and warming rate for the whole ocean (figure not shown) would eventually approach those in the 1-box model, given the same total ocean depth, the climate feedback in the two models and long enough time. Here, we see that under a constant γ (Fig. 5b), a decrease of the surface warming rate, i.e., a surface ocean hiatus, will never occur.

3.2 Varying efficiency of vertical heat transport

In reality, the surface ocean is usually warmed up faster than the deep ocean, leading to an enhanced vertical stratification at least during the transient period of global warming (Yang and Zhang 2008; Yang and Wang 2009). Although there is a lack of observational evidence supporting the proportional relationship between stratification and the efficiency of vertical heat transport, we can study a varying efficiency in a simple conceptual model, to gain insight to its role in surface warming hiatus. Here, we assume a linear relationship between the efficiency of vertical heat transport and vertical temperature gradient as follows,

$$\gamma = \gamma_0 + \beta T_v \tag{20}$$

where $\gamma_0 = 0.5\ W \bullet m^{-2}K^{-1}$ is the reference efficiency from an unperturbed state, and β is the rate of γ change, related to T_v. A positive β denotes a more (less) efficient vertical heat transport in response to an enhanced (weakened) stratification; and a negative β denotes a less (more) efficient vertical heat transport in response to an enhanced (weakened) stratification. Combining Eq. (20) with Eqs. (10, 11, 12), the 2-layer system becomes a cubic system. We can expect a third-order spline curve of the warming rate, with two turning points, when we solve this system numerically.

It is expected that an enhanced efficiency of vertical heat transport would slow down the surface warming to some extent, which is shown in Fig. 5d, e. For a strong positive $\beta(1\ W \bullet m^{-2}K^{-2})$, the surface ocean warming rate will reduce slightly after the fast transient period (Fig. 5e). However, the warming rate will restore and increase to the control level during the slow evolution stage of the deep ocean (red curve, Fig. 5e). To understand the behaviors of surface ocean warming rate, it is useful to examine the time differential equation of Eq. (10):

$$C_1\frac{d^2T_1}{dt^2} = \varepsilon - B\frac{dT_1}{dt} - \gamma_0\frac{d(T_1-T_2)}{dt} - 2\beta\left(T_1-T_2\right)\frac{d(T_1-T_2)}{dt} \tag{21}$$

Equation (21) indicates that the change of surface ocean warming rate is determined by external forcing ε, and by changes in climate feedback $-B\frac{dT_1}{dt}$, linear OHU $-\gamma_0\frac{d(T_1-T_2)}{dt}$ and quadratic OHU $-2\beta\left(T_1-T_2\right)\frac{d(T_1-T_2)}{dt}$. The contributions of these physical processes (right-hand side terms in Eq. (21)) to the warming rate change can be easily quantified.

In the beginning when the temperature change in the deep ocean is small, the stratification is enhanced with time, leading to a higher efficiency of downward heat transport, and thus a slightly reduced warming rate in the upper ocean. Figure 6 shows the time series of the terms in Eq. (21). In Fig. 5e, $\frac{dT_1}{dt}$ reaches a maximum in about 50 years; hence, its change rate $\frac{d^2T_1}{dt^2}$ is zero (black curve, Fig. 6a). This is determined by the strong negative climate feedback (solid red curve) and the heat uptake by the lower ocean (solid and dashed blue curves, Fig. 6a). In particular, the reduced warming rate during years 50 and 100, that is, the slightly negative $\frac{d^2T_1}{dt^2}$, is mainly due to the enhanced nonlinear OHU related to the β effect (dashed blue curve, Fig. 6a), because the other two terms are weakened slightly in this period. During this period, although the vertical stratification is still increasing (red curve, Fig. 5f), its rate of change is weakened. Therefore, the rate of linear OHU becomes weaker (solid blue curve, Fig. 6a), while the rate of quadratic OHU becomes stronger (dashed blue curve, Fig. 6a), leading to a negative $\frac{d^2T_1}{dt^2}$ (solid black curve, Fig. 6a). This state of affair cannot last very long because as $\frac{dT_1}{dt}$ decreases, it begins to close the gap between $\frac{dT_1}{dt}$ and $\frac{dT_2}{dt}$; specifically, it reduces the rate of linear OHU further (solid blue curve, Fig. 6a), which soon halts the decline of $\frac{dT_1}{dt}$ and makes it positive again. Note that it is the decrease of linear OHU after year 100 that makes the surface warming rate rise again, since the quadratic OHU continues to increase until about year 200. To better understand the role of the linear and nonlinear OHU in the surface warming, we also plot the terms of Eq. (21) with $\beta = 0$ in Fig. 6b. It is clear that without the quadratic OHU by the lower ocean, the surface ocean warming rate would never decline.

In the late stage of the surface ocean warming, the warming rate approaches the equilibrium in about 1000 years, mainly due to the enhanced climate feedback (solid red

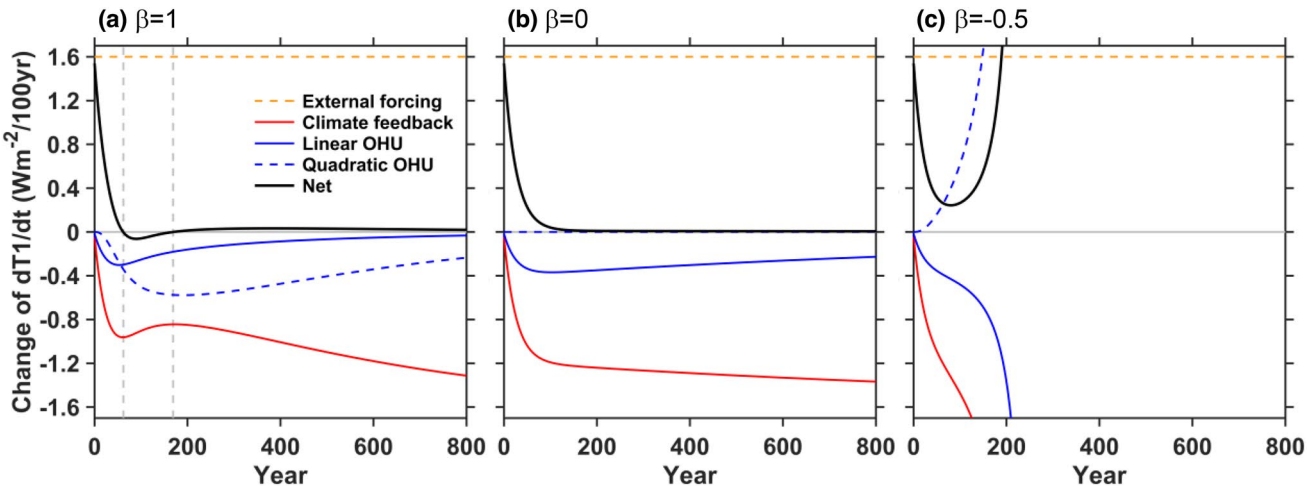

Fig. 6 Temporal changes of ocean heat content changing rate (units: $W \bullet m^{-2}(100yr)^{-1}$). The terms are calculated based on Eq. (21). Black curve is for the net $C_1\frac{d^2T_1}{dt^2}$; dashed orange curve, for external forcing ε; red curve, for linear climate feedback $-B\frac{dT_1}{dt}$; solid blue curve, for linear ocean heat uptake (OHU) by the lower ocean $-\gamma_0\frac{d(T_1-T_2)}{dt}$; and dashed blue curve, for quadratic OHU $-\beta\frac{d(T_1-T_2)^2}{dt}$. (**a**) $\gamma_0 = 0.5, \beta = 1$; (**b**) $\gamma_0 = 0.5, \beta = 0$; and (**c**) $\gamma_0 = 0.5, \beta = -0.5$

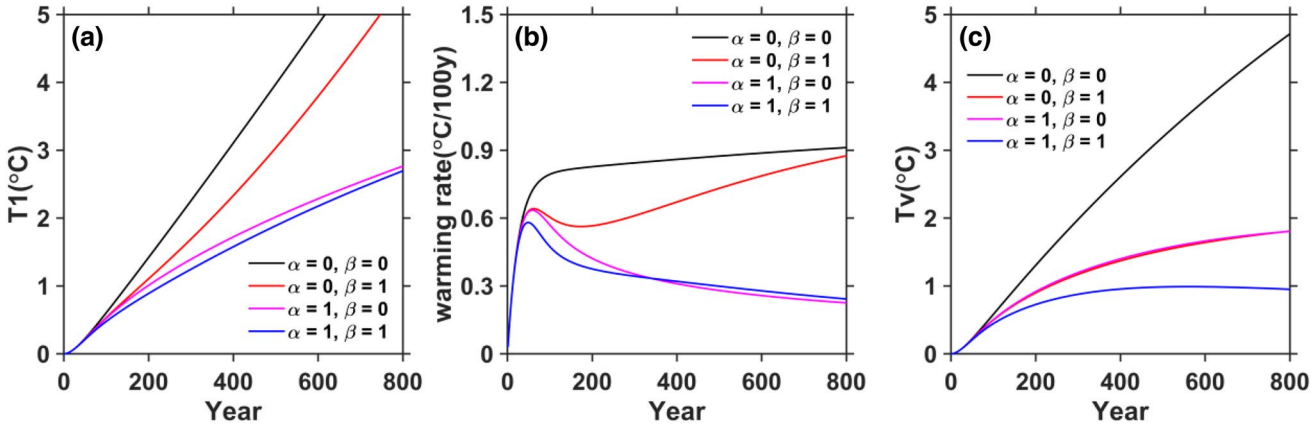

Fig. 7 Same as Fig. 5d–f, except for considering both enhanced negative climate feedback and vertical heat transport simultaneously in the 2-box model. Black and red curves are the same as those in Fig. 5d–f. Purple curve is for the case with only enhanced negative feedback ($\alpha = 1, \beta = 0$). Blue curve is for the case with both enhanced negative feedback and vertical heat transport ($\alpha = 1, \beta = 1$)

curve, Fig. 6a, b). The upper ocean is still transporting heat downward to the lower ocean, but at a very weak rate (blue curve, Fig. 6a, b). There is no upward heat release from the lower ocean because both the linear and quadratic OHU are negative (positive) for the upper (lower) ocean.

Note that the contributions of processes on the right-hand side of Eq. (21) to the warming rate change depend on the parameters of the system, such as B, γ_0, β, C_1, C_2, and so on. We examined large ranges of the parameters and their effects on the change of surface ocean warming rate (figures not shown). The common features we obtained are as follows: First, it is the enhanced nonlinear OHU (if it occurs in the ocean) that leads to a short-lived decline in the surface warming rate (i.e., negative $\frac{d^2T_1}{dt^2}$) during the first several decades of global warming, and second, it is the changing climate feedback that makes the warming rate approach the equilibrium in the long run.

The consequence for a negative β, i.e., a weaker efficiency for a stronger stratification, is straightforward. The surface warming rate, vertical temperature gradient and surface climate will explode, that is, the runaway climate would become inevitable, which would occur much faster than expected. This situation is shown by the blue curve in Fig. 5d–f, in which β is set to $-0.5\, W \bullet m^{-2}K^{-2}$. The quadratic OHU under this situation plays a dominant role in transporting heat upward from the lower ocean, contributing greatly to the exploding rise of surface warming rate (dashed blue curve, Fig. 6c), regardless of the strong stabilizing effects of the linear OHU and climate feedback (solid blue and red curves, Fig. 6c). We are not sure whether a negative β would be possible in reality. Considering the vast ocean and the complex bio-geo-chemical and physical processes in the real ocean, one cannot exclude the possibility that a negative β could occur.

3.3 Varying climate feedback and efficiency of vertical heat transport

If we consider both the enhanced negative feedback (Eq. (6)) and enhanced downward heat transport efficiency (Eq. (20)), the upper-ocean temperature Eq. (10) can be rewritten as follows,

$$C_1\frac{dT_1}{dt} = F - B_0T_1 - \gamma_0\left(T_1 - T_2\right) - \alpha T_1^2 - \beta\left(T_1 - T_2\right)^2 \tag{22}$$

And the time differential of Eq. (22) is,

$$\begin{aligned} C_1\frac{d^2T_1}{dt^2} &= \varepsilon - B_0\frac{dT_1}{dt} - \gamma_0\frac{d\left(T_1 - T_2\right)}{dt} \\ &- 2\alpha T_1\frac{dT_1}{dt} - 2\beta\left(T_1 - T_2\right)\frac{d(T_1 - T_2)}{dt} \end{aligned} \tag{23}$$

Equations (22, 23) can be easily solved numerically.

The surface warming can be reduced substantially, as expected (blue curve, Fig. 7a), under both the enhanced negative climate feedback and downward heat transport. Still, the surface warming hiatus (i.e., zero warming rate) would be unlikely to happen under a linearly increasing external forcing. For the surface ocean warming rate (Fig. 7b), the combined effect of enhanced climate feedback and downward heat transport (blue curve) is not the simple superimposition of enhanced climate feedback and downward heat transport (red and purple curves), due to strong nonlinear effects (Eq. (23)). In fact, the enhanced climate feedback (purple curve) appears to be more effective than the enhanced downward heat transport (red curve) to reduce the surface warming rate (Fig. 7b), since the former is determined by surface temperature (whose equilibrium rate of change is a constant), while the latter is determined

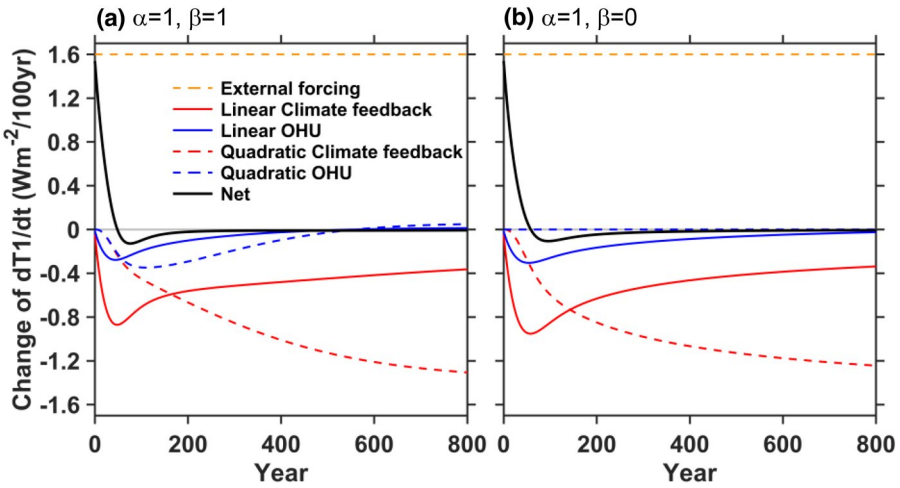

Fig. 8 Same as Fig. 6a, b, except for considering both enhanced negative climate feedback and vertical heat transport simultaneously in the 2-box model. The terms are calculated based on Eq. (23). Dashed red curve is for quadratic climate feedback $-\alpha\frac{dT_1^2}{dt}$. (**a**) $\alpha = 1, \beta = 1$ and (**b**) $\alpha = 1, \beta = 0$

by vertical temperature gradient (whose equilibrium rate of change is zero), as expressed in Eq. (23), under the condition of comparable parameters $\alpha \sim \beta$. Therefore, the magnitude of surface ocean warming is mainly determined by the climate feedback (purple and blue curves, Fig. 7a), which also plays a major role in determining vertical temperature gradient by controlling surface temperature (blue curve, Fig. 7c).

Different from the discussion in Sect. 3.2, in which the enhanced climate feedback is not considered, here the enhanced quadratic climate feedback can lead to a relatively long-lived decline in surface warming rate (blue curve in Fig. 7b, dashed red curve in Fig. 8). It will take a much longer time for the surface warming rate to approach the equilibrium due to the quadratic climate feedback. The effects from the other terms, in the long run, tend to always increase the warming rate (Fig. 8). In the presence of the quadratic climate feedback (dashed red curve, Fig. 8), the quadratic OHU plays a minor role in reducing the surface warming rate (dashed blue curve, Fig. 8), because the former depends only on surface warming, while the latter depends on vertical stratification, whose change will eventually approach zero.

Some studies suggested that the downward heat transport has contributed a great deal to the recent global warming hiatus. Watanabe et al. (2013) found ocean heat transport efficiency changes oppositely in general circulation models (GCMs) and in nature, namely, it is weakened in GCMs and strengthened in nature. The weakening tendency of γ in GCMs was seen in the concomitant transient experiments, in which CO_2 is increased at 1% per year, and also in individual models. These authors believed this can be the reason that GCMs tend to overestimate the surface warming trend. This is qualitatively consistent with our results with negative β (blue curve, Fig. 5e). England et al. (2014) also pointed out that anomalous winds can cause ocean energy redistribution, and thus induce a warming slowdown; however, rapid warming is expected to resume once the anomalous wind trend abates. This is in agreement with our results with positive β (red curve, Fig. 5). Although the triggering mechanisms are different in different studies and people tend to agree that the downward heat redistribution can slow down the surface warming rate, the hiatus induced by enhanced subsurface heat uptake cannot last long and surface temperature will eventually climb up. The 2-box model is quite simple; nevertheless, it captures the essential mechanism, which is qualitatively consistent with that from more complex coupled models and observational studies.

4 Conclusions and discussion

Inspired by the heated debate on the recent warming hiatus, we investigated two factors that could potentially mitigate GMST warming: the climate feedback of Earth system and ocean vertical heat mixing. The role of the climate feedback was studied using a 1-box EBM. It is shown that under the enhanced heating of GHGs, the GMST warming rate can be reduced if the global climate feedback becomes stronger. However, the warming hiatus appears to be unlikely, unless the global overall climate feedback goes to negative infinity. We realize that even under an extremely negative feedback, its damping effect on the global warming takes a long time to come into play and the magnitude is limited. Regardless of its simplicity, the 1-box EBM tells us that fundamentally, the climate feedback alone would never lead to a short-time hiatus, as observed in the first decades of the twenty-first century.

Under current global warming, the deep ocean, as an energy reservoir, is widely expected to curb the surface warming to some extent. Using a 2-box EBM, we found that the downward heat redistribution can indeed slow down the surface warming rate in the beginning; however,

the reduction induced by enhanced subsurface OHU cannot last long. In the long run, the surface warming will recover to be the same speed as that without the deep ocean heat uptake. The 2-box model is simple; nevertheless, it exhibits the essential processes of the vertical heat transport and deep ocean's roles in global warming. Results from this simple model are qualitatively consistent with those from observational studies and complex coupled modelling studies.

We need to be aware that in the real world, GMST change would never be as stable as shown in these simple models. It can be affected by volcano eruptions and other important aerosols, sunspot activities, cloud amount and distribution. Decadal temperature change can be even stronger than the long-term trend (Liebmann et al. 2010), so is the decadal climate feedback. Therefore, it is likely that the recent hiatus had some link to a more negative decadal-changed climate feedback, as suggested in Zhou et al. (2016). SST pattern-induced low-cloud anomalies are substantially more negative than the long-term cloud feedback, and could have contributed to the period of reduced warming between 1998 and 2013 (Zhou et al. 2016).

In the box models, several assumptions are used, which are simple but without loss of generality. For example, in the 1-box model we assumed a linear increase of the negative feedback with the increase of GMST, to test whether a stiffening-up of damping effect of the climate feedback could possibly lead to a hiatus. We found that a zero warming rate is not plausible under the linearly increasing external heating. In the 2-box model, the vertical heat transfer efficiency was assumed to change linearly with vertical temperature gradient. Thus, we found that a slowdown of the surface ocean warming will be surely followed by an acceleration of surface warming. The box models contain several important parameters, such as the climate feedback, vertical heat transfer coefficient, the thicknesses of the upper and lower oceans, etc. We tested wide ranges of values of these parameters, and they did not affect our conclusions qualitatively.

Results from simple box models provide further evidence that we should not be blinded by the short-term warming slowdown, as shown in the observations. The long-term trend of global warming cannot be undermined by the occurrence of a one-time, 15-year hiatus. The severity of climate change is closely tied to the total emissions due to anthropogenic activities since the Industrial Revolution, because the carbon dioxide is long lived in the atmosphere. Reducing the GHG emission is the most feasible solution to prevent the Earth from becoming too warm for humans to live on. And a quicker action is the better action.

Appendix

1. One-box model with varying climate feedback

Based on Eqs. (1), (2) and (6), the combined equation is:

$$\frac{dT}{dt} + aT^2 + bT = Kt \tag{A1}$$

This is Riccati equation, a nonlinear differential equation with constant coefficients of the first order. The parameters in (A1) are defined as follows,

$$a = \frac{\alpha}{C}, b = \frac{B_0}{C}, K = \frac{\varepsilon}{C}$$

To obtain the theoretical solution to (A1), we redefine $T = \frac{1}{a}\frac{F'}{F}$. Then, we have:

$$\frac{dT}{dt} = \frac{1}{a}\frac{F''F - F'^2}{F} = \frac{1}{a}\left[\frac{F''}{F} - \left(\frac{F'}{F}\right)^2\right] = \frac{1}{a}\frac{F''}{F} - aT^2$$

Therefore, (A1) can be rewritten as,

$$\frac{1}{a}\frac{F''}{F} - aT^2 + aT^2 + \frac{b}{a}\frac{F'}{F} = Kt$$

$$\frac{1}{a}\frac{F''}{F} + \frac{b}{a}\frac{F'}{F} = Kt$$

$$F'' + bF' - aKtF = 0 \tag{A2}$$

Eq. (A2) is a linear differential equation with variable coefficients of the second order.

If we define $F(t) = Z(t)e^{-\frac{b}{2}t}$, we have:

$$F' = (Z' - \frac{b}{2}Z)e^{-\frac{b}{2}t}$$

$$F'' = (Z'' - bZ' + \frac{b^2}{4}Z)e^{-\frac{b}{2}t}$$

$$\left(Z'' - bZ' + \frac{b^2}{4}Z\right)e^{-\frac{b}{2}t} + b \times \left(Z' - \frac{b}{2}Z\right)e^{-\frac{b}{2}t} - aKt \times Ze^{-\frac{b}{2}t} = 0$$

$$\left(Z'' - \frac{b^2}{4}Z - aKtZ\right)e^{-\frac{b}{2}t} = 0$$

$$Z'' - \left(\frac{b^2}{4} + aKt\right)Z = 0 \tag{A3}$$

We then define $M = m\left(\frac{b^2}{4} + aKt\right)$, where $m = (aK)^{-\frac{2}{3}}$. We have:

$$\frac{d^2Z}{dt^2} = (aKm)^2 \frac{d^2Z}{dM^2}$$

$$(aKm)^2 \frac{d^2Z}{dM^2} - \frac{M}{m}Z = 0$$

$$a^2K^2m^3 = a^2K^2(aK)^{-\frac{2}{3}\times 3} = 1$$

$$\frac{d^2Z}{dM^2} - MZ = 0 \tag{A4}$$

Eq. (A4) is Airy's Equation, which has two specific solutions:

$Z = A(0, M)$ or $A(2, M)$ where $A(0, M)$ and $A(2, M)$ represent two kinds of Airy function.

The general solution to Eq. (A4) is:

$$Z(t) = K_2A(0, M) + K_1A(2, M) \tag{A5}$$

Therefore, $F(t)$ can be expressed as follows:

$$F(t) = K_2e^{-\frac{b}{2}t}A(0, M) + K_1e^{-\frac{b}{2}t}A(2, M)$$

$$F'(t) = K_2\left[-\frac{b}{2}e^{-\frac{b}{2}t}A(0, M) + aKme^{-\frac{b}{2}t}A(1, M)\right] + K_1\left[-\frac{b}{2}e^{-\frac{b}{2}t}A(2, M) + aKme^{-\frac{b}{2}t}A(3, M)\right]$$

Substituting $F(t)$ into T, we have the expression of T:

$$T = \frac{1}{a}\frac{F'}{F} = \frac{K_2\left[-\frac{b}{2}e^{-\frac{b}{2}t}A(0, M) + aKme^{-\frac{b}{2}t}A(1, M)\right] + K_1\left[-\frac{b}{2}e^{-\frac{b}{2}t}A(2, M) + aKme^{-\frac{b}{2}t}A(3, M)\right]}{a[K_2e^{-\frac{b}{2}t}A(0, M) + K_1e^{-\frac{b}{2}t}A(2, M)]} = \frac{-\frac{b}{2}A(0, M) + aKmA(1, M) - \frac{K_1}{K_2}\frac{b}{2}A(2, M) + \frac{K_1}{K_2}aKmA(3, M)}{a[A(0, M) + \frac{K_1}{K_2}A(2, M)]} = \frac{aKm\left[A(1, M) + \frac{K_1}{K_2}A(3, M)\right] - \frac{b}{2}\left[A(0, M) + \frac{K_1}{K_2}A(2, M)\right]}{a[A(0, M) + \frac{K_1}{K_2}A(2, M)]} \tag{A6}$$

Since the initial condition is $T(0) = 0$, we have $F'(0) = 0$, that is,

$$F'(0) = K_2\left[-\frac{b}{2}A\left(0, \frac{b^2m}{4}\right) + aKmA\left(1, \frac{b^2m}{4}\right)\right] + K_1\left[-\frac{b}{2}A\left(2, \frac{b^2m}{4}\right) + aKmA\left(3, \frac{b^2m}{4}\right)\right] = 0$$

$$\left[-\frac{b}{2}A\left(0, \frac{b^2m}{4}\right) + aKmA\left(1, \frac{b^2m}{4}\right)\right] + \frac{K_1}{K_2}\left[-\frac{b}{2}A\left(2, \frac{b^2m}{4}\right) + aKmA\left(3, \frac{b^2m}{4}\right)\right] = 0$$

Therefore,

$$\frac{K_1}{K_2} = \frac{\frac{b}{2}A\left(0, \frac{b^2m}{4}\right) - aKmA\left(1, \frac{b^2m}{4}\right)}{-\frac{b}{2}A\left(2, \frac{b^2m}{4}\right) + aKmA\left(3, \frac{b^2m}{4}\right)} \tag{A7}$$

The definitions of K_1 and K_2 are given as follows:

$$\begin{aligned} K_1 &= \frac{b}{2}A\left(0, \frac{b^2m}{4}\right) - aKmA\left(1, \frac{b^2m}{4}\right) \\ K_2 &= -\frac{b}{2}A\left(2, \frac{b^2m}{4}\right) + aKmA\left(3, \frac{b^2m}{4}\right) \end{aligned},$$

2. Two-box model with constant efficiency of vertical heat transport

Equations (10, 11) give the first-order nonhomogeneous linear differential equation system, which can be rewritten in the matrix form as follows:

$$\boldsymbol{T}'(t) - \boldsymbol{A}\boldsymbol{T}(t) = \boldsymbol{b}(t) \tag{A8}$$

where.

$$\boldsymbol{T}(t) = \begin{pmatrix} T_1 \\ T_2 \end{pmatrix}, \boldsymbol{A} = \begin{pmatrix} -\frac{B+\gamma}{C_1} & \frac{\gamma}{C_1} \\ \frac{\gamma}{C_2} & -\frac{\gamma}{C_2} \end{pmatrix} \text{ and } \boldsymbol{b}(t) = \begin{pmatrix} \frac{\varepsilon}{C_1}t \\ 0 \end{pmatrix}.$$

The associated homogeneous system to (A8) is $\boldsymbol{T}'(t) - \boldsymbol{A}\boldsymbol{T}(t) = 0$

The eigen equation of the homogeneous system is:

$$p(\lambda) = |\boldsymbol{A} - \lambda I| = \begin{pmatrix} -\frac{B+\gamma}{C_1} - \lambda & \frac{\gamma}{C_1} \\ \frac{\gamma}{C_2} & -\frac{\gamma}{C_2} - \lambda \end{pmatrix} = \left(\frac{B+\gamma}{C_1} + \lambda\right)\left(\frac{\gamma}{C_2} + \lambda\right) - \frac{\gamma^2}{C_1 C_2} = 0 \tag{A9}$$

where λ is the eigenvalue of $\boldsymbol{A}$. The equation for λ can be simplified as follows,

$$\lambda^2 + b\lambda + \frac{\gamma B}{C_1 C_2} = 0 \tag{A10}$$

where $b = \frac{B+\gamma}{C_1} + \frac{\gamma}{C_2}$. Eq. (A10) has real solutions,

$$\lambda_{1,2} = \frac{-b \pm \sqrt{\delta}}{2}, and, \delta = b^2 - 4\frac{\gamma B}{C_1 C_2} > 0 \tag{A11}$$

By defining $b^* = \frac{B+\gamma}{C_1} - \frac{\gamma}{C_2}$, we have.

$p(\lambda) = \begin{pmatrix} \frac{-b^*-\sqrt{\delta}}{2} & \frac{\gamma}{C_1} \\ \frac{\gamma}{C_2} & \frac{b^*-\sqrt{\delta}}{2} \end{pmatrix} \sim \begin{pmatrix} \frac{-b^*-\sqrt{\delta}}{2} & \frac{\gamma}{C_1} \\ 0 & 0 \end{pmatrix}$, when $\lambda = \frac{-b+\sqrt{\delta}}{2}$

$p(\lambda) = \begin{pmatrix} \frac{-b^*+\sqrt{\delta}}{2} & \frac{\gamma}{C_1} \\ \frac{\gamma}{C_2} & \frac{b^*+\sqrt{\delta}}{2} \end{pmatrix} \sim \begin{pmatrix} \frac{-b^*+\sqrt{\delta}}{2} & \frac{\gamma}{C_1} \\ 0 & 0 \end{pmatrix}$, when $\lambda = \frac{-b-\sqrt{\delta}}{2}$

Therefore, the associated eigenvectors can be expressed as follows,

$$\boldsymbol{v}_1 = \begin{pmatrix} 1 \\ \varphi_f \end{pmatrix}, \boldsymbol{v}_2 = \begin{pmatrix} 1 \\ \varphi_s \end{pmatrix} \tag{A12}$$

where,

$$\varphi_f = \frac{C_1}{2\gamma}\left(b^* - \sqrt{\delta}\right) and, \varphi_s = \frac{C_1}{2\gamma}(b^* + \sqrt{\delta})$$

The e-folding timescale is defined by,

$$\tau = -\frac{1}{\lambda_{1,2}} = -\frac{2}{-b \pm \sqrt{\delta}} = \frac{C_1 C_2}{2B\gamma}(b \pm \sqrt{\delta})$$

Therefore, we have the fast timescale τ_f and slow timescale τ_s, as follows,

$\tau_f = \frac{C_1 C_2}{2B\gamma}(b - \sqrt{\delta})$, and $\tau_s = \frac{C_1 C_2}{2B\gamma}(b + \sqrt{\delta})$

The fundamental matrix based on (A12) is:

$$\Phi(t) = (\boldsymbol{v}_1 e^{\lambda_1 t} \ \boldsymbol{v}_2 \, e^{\lambda_2 t}) = \begin{pmatrix} e^{-\frac{t}{\tau_f}} & e^{-\frac{t}{\tau_s}} \\ \varphi_f e^{-\frac{t}{\tau_f}} & \varphi_s e^{-\frac{t}{\tau_s}} \end{pmatrix} \tag{A13}$$

The general solution to this homogeneous system is

$\boldsymbol{T_c}(t) = \Phi(t)\boldsymbol{K}$

where $\boldsymbol{K} = \begin{pmatrix} K_1 \\ K_2 \end{pmatrix}$ is a matrix with undetermined coefficients.

A particular solution is given by the expression:

$$\boldsymbol{T_p}(t) = \Phi(t) \int \Phi(t)^{-1}\boldsymbol{b}(t)dt$$

Substituting with $\Phi(t)$ and $\boldsymbol{b}(t)$, we obtain

$$\Phi(t)^{-1}\boldsymbol{b}(t) = \frac{\Phi^*(t)}{|\Phi(t)|}\boldsymbol{b}(t) = \begin{pmatrix} \varphi_s e^{-\frac{t}{\tau_s}} & -e^{-\frac{t}{\tau_s}} \\ -\varphi_f e^{-\frac{t}{\tau_f}} & e^{-\frac{t}{\tau_f}} \end{pmatrix} \frac{e^{\left(\frac{1}{\tau_s}+\frac{1}{\tau_f}\right)t}}{\varphi_s - \varphi_f} \times \begin{pmatrix} \frac{\varepsilon}{C_1}t \\ 0 \end{pmatrix}$$

$$= \frac{e^{\left(\frac{1}{\tau_s}+\frac{1}{\tau_f}\right)t}}{\varphi_s - \varphi_f}\begin{pmatrix} \frac{\varepsilon}{C_1}t \times \varphi_s e^{-\frac{t}{\tau_s}} \\ \frac{\varepsilon}{C_1}t \times (-\varphi_f e^{-\frac{t}{\tau_f}}) \end{pmatrix} = \frac{\frac{\varepsilon}{C_1}}{\varphi_s - \varphi_f}\begin{pmatrix} \varphi_s t e^{\frac{t}{\tau_f}} \\ -\varphi_f t e^{\frac{t}{\tau_s}} \end{pmatrix}$$

Therefore, the expression of T_p can be written as

$$\boldsymbol{T_p}(t) = \Phi(t) \int \Phi(t)^{-1}\boldsymbol{b}(t)dt = \begin{pmatrix} e^{-\frac{t}{\tau_f}} & e^{-\frac{t}{\tau_s}} \\ \varphi_f e^{-\frac{t}{\tau_f}} & \varphi_s e^{-\frac{t}{\tau_s}} \end{pmatrix} \frac{\varepsilon}{C_1(\varphi_s - \varphi_f)}\begin{pmatrix} \varphi_s \int t e^{\frac{t}{\tau_f}}dt \\ -\varphi_f \int t e^{\frac{t}{\tau_s}}dt \end{pmatrix}$$

Here,

$$\int t e^{\frac{t}{\tau_f}}dt = \tau_f \int t de^{\frac{t}{\tau_f}} = \tau_f\left(t e^{\frac{t}{\tau_f}} - \int e^{\frac{t}{\tau_f}}dt\right) = \tau_f e^{\frac{t}{\tau_f}}\left(t - \tau_f\right)$$

Therefore, T_p can be written as:

$$\boldsymbol{T_p}(t) = \frac{\varepsilon}{B}\begin{pmatrix} a_f(t-\tau_f) + a_s(t-\tau_s) \\ \varphi_f a_f(t-\tau_f) + \varphi_s a_s(t-\tau_s) \end{pmatrix} \tag{A14}$$

where the fast and slow parameters of a_f and a_s are defined, respectively, as follows,

$a_f = \frac{\varphi_s \tau_f}{C_1(\varphi_s - \varphi_f)}B$ and $a_s = -\frac{\varphi_f \tau_s}{C_1(\varphi_s - \varphi_f)}B$

Consider the following identities,

$$a_s + a_f = \frac{B}{C_1(\varphi_s - \varphi_f)}\left(-\varphi_f \tau_s + \varphi_s \tau_f\right) = \frac{1}{\varphi_s - \varphi_f}\frac{C_1 C_2}{4\gamma^2} \times 2\sqrt{\delta}(b - b^*) = 1$$

$$\varphi_f a_f + \varphi_s a_s = \frac{B\varphi_s\varphi_f}{C_1(\varphi_s - \varphi_f)}(\tau_f - \tau_s) = -\frac{C_2}{C_1}\left(\frac{C_1}{2\gamma}\right)^2 \left[b^{*2} - \left(b^2 - 4\frac{B\gamma}{C_1 C_2}\right)\right] = 1$$

Therefore, T_p can be finally re-written as follows:

$$\boldsymbol{T_p}(t) = \frac{\varepsilon}{B}\begin{pmatrix} t - (a_f\tau_f + a_s\tau_s) \\ t - (\varphi_f a_f \tau_f + \varphi_s a_s \tau_s) \end{pmatrix} \tag{A15}$$

The general solution to the nonhomogeneous equation consists of the general solution to the homogeneous equation and a particular solution to the nonhomogeneous equation. Therefore, the expression of the solution $\boldsymbol{T}(t)$ can be written as

$$\boldsymbol{T}(t) = \Phi(t)\boldsymbol{K} + \boldsymbol{T_p}(t) = \begin{pmatrix} e^{-\frac{t}{\tau_f}} & e^{-\frac{t}{\tau_s}} \\ \varphi_f e^{-\frac{t}{\tau_f}} & \varphi_s e^{-\frac{t}{\tau_s}} \end{pmatrix}\boldsymbol{K} + \frac{\varepsilon}{B}\begin{pmatrix} a_f(t-\tau_f) + a_s(t-\tau_s) \\ \varphi_f a_f(t-\tau_f) + \varphi_s a_s(t-\tau_s) \end{pmatrix} \tag{A16}$$

Consider the initial conditions $\boldsymbol{T} = \begin{pmatrix} 0 \\ 0 \end{pmatrix}$, $att = 0$, we have.

$$\boldsymbol{T}(0) = \begin{pmatrix} 1 & 1 \\ \varphi_f & \varphi_s \end{pmatrix}\begin{pmatrix} K_1 \\ K_2 \end{pmatrix} + \frac{\varepsilon}{B}\begin{pmatrix} -\tau_f a_f - \tau_s a_s \\ -\tau_f\varphi_f a_f - \tau_s\varphi_s a_s \end{pmatrix} = \begin{pmatrix} 0 \\ 0 \end{pmatrix}$$

Therefore,

$$\begin{cases} K_1 = \frac{\varepsilon}{B}\frac{1}{\varphi_s - \varphi_f}(\tau_f\varphi_s a_f + \tau_s\varphi_s a_s - \tau_f\varphi_f a_f - \tau_s\varphi_s a_s) = \frac{\varepsilon}{B}\tau_f a_f \\ K_2 = -\frac{\varepsilon}{B}\frac{1}{\varphi_s - \varphi_f}(\tau_f\varphi_f a_f + \tau_s\varphi_f a_s - \tau_f\varphi_f a_f - \tau_s\varphi_s a_s) = \frac{\varepsilon}{B}\tau_s a_s \end{cases} \tag{A17}$$

Substituting (A17) into (A16), we have

$$\boldsymbol{T}(t) = \frac{\varepsilon}{B}\begin{pmatrix} t - \tau_f a_f\left(1 - e^{-\frac{t}{\tau_f}}\right) - \tau_s a_s(1 - e^{-\frac{t}{\tau_s}}) \\ t - \varphi_f\tau_f a_f\left(1 - e^{-\frac{t}{\tau_f}}\right) - \varphi_s\tau_s a_s(1 - e^{-\frac{t}{\tau_s}}) \end{pmatrix} \tag{A18}$$

Finally, we obtain the solutions to T_1 and T_2,

$$T_1(t) = \frac{\varepsilon}{B}\left[t - \tau_f a_f\left(1 - e^{-\frac{t}{\tau_f}}\right) - \tau_s a_s\left(1 - e^{-\frac{t}{\tau_s}}\right)\right] \tag{A19}$$

$$T_2(t) = \frac{\varepsilon}{B}\left[t - \varphi_f\tau_f a_f\left(1 - e^{-\frac{t}{\tau_f}}\right) - \varphi_s\tau_s a_s\left(1 - e^{-\frac{t}{\tau_s}}\right)\right] \tag{A20}$$

And the vertical temperature difference T_v is:

$$T_v(t) = T_1 - T_2 = \frac{\varepsilon}{B}\left[(\varphi_f - 1)\tau_f a_f\left(1 - e^{-\frac{t}{\tau_f}}\right) + (\varphi_s - 1)\tau_s a_s\left(1 - e^{-\frac{t}{\tau_s}}\right)\right] \tag{A21}$$

Funding Funding was provided by the National Nature Science Foundation of China (41725021, 91737204 and 41376007) and the National Key Research and Development Program of China (2016YFA0601802).

Data Availability Not applicable.

References

Abramowitz M, Stegun IA (1964) Handbook of mathematical functions with formulas graphs mathematical tables. US Government printing office, 446–452.

Armour KC, Bitz CM, Roe GH (2013) Time-varying climate sensitivity from regional feedbacks. J Clim 26:4518–4534

Balmaseda MA, Mogensen K, Weaver AT (2013a) Evaluation of the ECMWF ocean reanalysis system ORAS4. Q J R Meteorol Soc 139:1132–1161

Balmaseda MA, Trenberth KE, Källén E (2013b) Distinctive climate signals in reanalysis of global ocean heat content. Geophys Res Lett 40:1754–1759

Bloch-Johnson J, Pierrehumbert RT, Abbot DS (2015) Feedback temperature dependence determines the risk of high warming. Geophys Res Lett 42:4973–4980

Bony S, Colman R, Kattsov VM, Allan RP, Bretherton CS, Dufresne JL, Hall A, Hallegatte S, Holland MM, Ingram W, Randall DA (2006) How well do we understand evaluate climate change feedback processes? J Clim 19:3445–3482

Brown PT, Li W, Xie SP (2015) Regions of significant influence on unforced global mean surface air temperature variability in climate models. J Geophys Res Atmos 120:480–494

Chen X, Tung KK (2014) Varying planetary heat sink led to global-warming slowdown acceleration. Science 345:897–903

Chen X, Tung KK (2018) Global surface warming enhanced by weak Atlantic overturning circulation. Nature 559:387–391

Clement A, DiNezio P (2014) The tropical Pacific Ocean—Back in the driver's seat? Science 343:976–978

Dai A, Fyfe JC, Xie SP, Dai X (2015) Decadal modulation of global surface temperature by internal climate variability. Nat Clim Chang 5:555–559

Drijfhout SS, Blaker AT, Josey SA, Nurser AJG, Sinha B, Balmaseda MA (2014) Surface warming hiatus caused by increased heat uptake across multiple ocean basins. Geophys Res Lett 4(22):7868–7874. https://doi.org/10.1002/2014GL061456

Easterling DR, Wehner MF (2009) Is the climate warming or cooling? Geophys Res Lett 36:2

England MH, Mcgregor S, Spence P, Meehl GA, Timmermann A, Cai W et al (2014) Recent intensification of wind-driven circulation in the Pacific and the ongoing warming hiatus. Nat Clim Chang 4:222–227

Geoffroy O, Saint-Martin D, Olivié DJ, Voldoire A, Bellon G, Tytéca S (2013) Transient climate response in a two-layer energy-balance model. Part I: analytical solution parameter calibration using CMIP5 AOGCM experiments. J Clim 26:1841–1857

Gregory JM (2000) Vertical heat transports in the ocean and their effect on time-dependent climate change. Clim Dyn 16:501–515

Gregory JM, Mitchell JF (1997) The climate response to CO2 of the Hadley Centre coupled AOGCM with and without flux adjustment. Geophys Res Lett 24:1943–1946

Gregory JM, Ingram WJ, Palmer MA, Jones GS, Stott PA, Thorpe RB, Lowe JA, Johns TC, Williams KD (2004) A new method for diagnosing radiative forcing and climate sensitivity. Geophys Res Lett 31:2

Gregory JM, Rews T, Good P (2015) The inconstancy of the transient climate response parameter under increasing CO2. Philos Trans R Soc A Math Phys Eng Sci 373:2

Hansen J, Johnson D, Lacis A, Lebedeff S, Lee P, Rind D, Russell G (1981) Climate impact of increasing atmospheric carbon dioxide. Science 213:957–966

Held IM, Winton M, Takahashi K, Delworth T, Zeng F, Vallis GK (2010) Probing the fast and slow components of global warming by returning abruptly to preindustrial forcing. J Clim 23:2418–2427

IPCC (2013) Climate change 2013: the physical science basis. Cambridge University Press, Cambridge, p 1535

Jones PD, Lister DH, Osborn TJ, Harpham C, Salmon M, Morice CP (2012) Hemispheric and large-scale land surface air temperature variations: an extensive revision and an update to 2010. J Geophys Res. https://doi.org/10.1029/2011JD017139

Kaufmann RK, Kauppi H, Mann ML, Stock JH (2011) Reconciling anthropogenic climate change with observed temperature 1998–2008. Proc Natl Acad Sci 108:11790–11793

Knight J, Kennedy J, Folland C, Harris G, Jones GS, Palmer M, Parker D, Scaife A, Stott P (2009) Global oceans: Do global temperature trends over the last decade falsify climate predictions? Bull Am Meteorol Soc 90:56–57

Kosaka Y, Xie SP (2013) Recent global-warming hiatus tied to equatorial Pacific surface cooling. Nature 501:403–407

Kühn T, Partanen AI, Laakso A, Lu Z, Bergman T, Mikkonen S, Kokkola H, Korhonen H, Räisänen P, Streets DG, Romakkaniemi S (2014) Climate impacts of changing aerosol emissions since 1996. Geophys Res Lett 41:4711–4718

Liebmann B, Dole RM, Jones C, Bladé I, Allured D (2010) Influence of choice of time period on global surface temperature trend estimates. Bull Am Meteorol Soc 91:1485–1492

Liu W, Xie SP, Lu J (2016) Tracking ocean heat uptake during the surface warming hiatus. Nat Commun 7:1–9

Loeb NG, Lyman JM, Johnson GC, Allan RP, Doelling DR, Wong T, Soden BJ, Stephens GL (2012) Observed changes in top-of-the-atmosphere radiation and upper-ocean heating consistent within uncertainty. Nat Geosci 5:110–113

Manabe S, Bryan K (1985) CO2-induced change in a coupled ocean-atmosphere model and its paleoclimatic implications. J Geophys Res 90:11689–11707

Meehl GA, Arblaster JM, Fasullo JT, Hu A, Trenberth KE (2011) Model-based evidence of deep-ocean heat uptake during surface-temperature hiatus periods. Nat Clim Chang 1:360–364

Meehl GA et al (2013) Climate change projections in CESM1 (CAM5) compared to CCSM4. J Clim 26:6287–6308

Morice CP, Kennedy JJ, Rayner NA, Jones PD (2012) Quantifying uncertainties in global and regional temperature change using an ensemble of observational estimates: the HadCRUT4 dataset. J Geophys Res 117:D08101. https://doi.org/10.1029/2011JD017187

Raper SCB, Gregory JM, Stouffer RJ (2002) The role of climate sensitivity and ocean heat uptake on AOGCM transient temperature response. J Clim 15:124–130

Rhein M et al (2013) Observations: ocean in climate change 2013: the physical science basis. Cambridge Univ Press, Cambridge, pp 255–316

Roe GH, Armour KC (2011) How sensitive is climate sensitivity? Geophys Res Lett 38:L14708. https://doi.org/10.1029/2011GL047913

Rugenstein M, Bloch-Johnson J, Gregory JM, Mauritsen T, Li C, Frölicher TL, Paynter D, Danabasoglu G, Yang S, Dufresne JL (2020) Equilibrium climate sensitivity estimated by equilibrating climate models. Geophys Res Lett 47:e2019

Santer BD, Bonfils C, Painter JF, Zelinka MD, Mears C, Solomon S, Schmidt GA, Fyfe JC, Cole JN, Nazarenko L, Taylor KE (2014) Volcanic contribution to decadal changes in tropospheric temperature. Nat Geosci 7:185–189

Schmidt GA, Shindell DT, Tsigaridis K (2014) Reconciling warming trends. Nat Geosci 7:158–160

Smith D, Booth B, Dunstone N et al (2016) Role of volcanic and anthropogenic aerosols in the recent global surface warming slowdown. Nat Clim Chang 6:936–940. https://doi.org/10.1038/nclimate3058

Soden BJ, Held IM (2006) An assessment of climate feedbacks in coupled ocean–atmosphere models. J Clim 19:3354–3360

Solomon S, Rosenlof KH, Portmann RW et al (2010) Contributions of stratospheric water vapor to decadal changes in the rate of global warming. Science 327:1219–1223. https://doi.org/10.1126/science1182488

Trenberth KE (2009) An imperative for adapting to climate change: tracking Earth's global energy. Curr Opin Environ Sustain 1:19–27

Trenberth KE, Fasullo JT (2013) An apparent hiatus in global warming? Earths Fut. 1:19–32

Tung KK, Chen X (2018) Understanding the recent global surface warming slowdown: a review. Climate 6:82

Watanabe M, Kamae Y, Yoshimori M, Oka A, Sato M, Ishii M et al (2013) Strengthening of ocean heat uptake efficiency associated with the recent climate hiatus. Geophys Res Lett 40:3175–3179

Winton M, Takahashi K, Held IM (2010) Importance of ocean heat uptake efficacy to transient climate change. J Clim 23:2333–2344

Xie SP, Kosaka Y, Okumura YM (2016) Distinct energy budgets for anthropogenic and natural changes during global warming hiatus. Nature Geosci 9:29–33

Yan XH, Boyer T, Trenberth K, Karl TR, Xie SP, Nieves V, Tung KK, Roemmich D (2016) The global warming hiatus: slowdown or redistribution? Earth's Future 4:472–482

Yang H, Wang F (2009) Revisiting the thermocline depth in the equatorial Pacific. J Clim 22:3856–3863

Yang H, Zhang Q (2008) Anatomizing the ocean role in ENSO changes under global warming. J Clim 21:6539–6555. https://doi.org/10.1175/2008JCLI2324.1

Yoshimori M, Masahiro W et al (2016) A review of progress towards understanding the transient global mean surface temperature response to radiative perturbation. Progr Earth Planetary Sci 3:2

Zhou T, Chen X (2015) Uncertainty in the 2 °C warming threshold related to climate sensitivity and climate feedback. J Meteorol Res 29:884–895

Zhou C, Zelinka MD, Klein SA (2016) Impact of decadal cloud variations on the Earth's energy budget. Nat Geosci 9:871–874